



THE IMPACT OF DISTORTED INFLOW ON A CENTRIFUGAL FAN NOISE

Joachim DOMINIQUE ¹, Julien CHRISTOPHE ¹, Olivier CHERIAUX ²,
Fabrice AILLOUD ², Manuel HENNER ², Christophe SCHRAM ¹

¹ *von Karman Institute, 72 Chaussée de Waterloo,
1640 Rhode-Saint-Genèse, Belgique*

² *Valeo Thermique Habitacle, 8 rue Louis Lormand.
78321 La Verrière, France*

SUMMARY

Small ducted fans in HVAC applications are often affected by their integration within the final product. The flow and operating conditions induced by the fan working environment significantly impact its noise emission and aerodynamic performances. This paper presents a combined numerical/experimental approach using LES simulations and multi-ports measurements to investigate such installation effects for a centrifugal fan subjected to distorted inflow conditions. We observe that the distortion increases the fan broadband noise while suppressing its tonal emissions and we attribute those changes to the lack of constructive interference between individual blades' forces in distorted inflows.

INTRODUCTION

If only 12 % of passengers' cars are electric vehicles in 2020, this sector is expected to grow rapidly as the European Union proposes to ban new internal combustion vehicles from 2035 to reduce CO₂ emissions. This transition dramatically changes the background noise level perceived in the car cabin. The internal combustion engine noise is no longer the primary noise source, which is now dominated by the Heating, Ventilation and Air Conditioning (HVAC) and the tires and terrain [1, 2].

The noise generated by an HVAC system is caused mainly by the fan noise emission and its transmission through the duct system situated within the dashboard. Car manufacturers are nowadays able to design low noise HVAC fans. Still, the integration of the fan within the compact ventilation system of the vehicle can often lead to undesirable noise increases and so-called *installation effects*.

Unfortunately, installation effects are complex and difficult to estimate. Firstly, the non-uniformity of the flow ingested by the fan can change the unsteady aerodynamic forces acting on the blades and the fan casing, which are the dominant sources of noise for fans at low Mach number [3]. Secondly, the installation of the fan within the circuit can change the fan operating conditions [4]. Finally, the scattering of the acoustic field by the duct system can impact the radiation efficiency of the fan [5]. Those complex installation effects mainly depend on the fan inflow, which can significantly change its overall noise emission, and are still not well understood.

Fan noise is usually composed of a tonal and broadband component. Mugridge [6] and Sturn [7] showed that the tone at the blade passing frequency could be attributed to atmospheric turbulence ingestion. Lee [8] linked the tones amplitude and their frequency to the length scale of the ingested turbulent eddies showing that eddies smaller than the blade chords could cause sub-harmonic tones. Kromer [9] measured the noise emitted by axial fans with inflow distortions grids to generate turbulence and non-uniform inflows. An increase in tonal sound was associated with elevated unsteady blade forces caused by increased turbulence and inhomogeneous inflow conditions. The broadband sound emission was attributed to an increase in turbulence ingestion noise. However, all investigations were performed on axial fans. In contrast, the impact of non-uniform and turbulent inflow on centrifugal fan noise remains largely unexplored and is considered in this work.

The remaining of the paper is structured as follows. In the first section, the experimental methodology employed to measure the centrifugal fan noise is shortly described, and fan noise emissions under different inflows are compared. The second section is dedicated to the description of the numerical model based on LES simulations. The last section investigates the forces acting on the fan's blades as a dominant noise source and we observe the similarities between the blade's loading and measured acoustic emissions in different inflows.

EXPERIMENTS

The measurements are performed in the ALCOVES anechoic wind tunnel of the von Karman Institute for Fluid Dynamics (VKI). This wind tunnel comprises two anechoic rooms separated by a modular wall panel. An external fan controls the pressure difference between the rooms and, therefore, the operating condition of the centrifugal fan investigated within the duct.

As illustrated in Fig. 1, a duct of 15 cm inner diameter is instrumented with two microphone stations on both sides of the fan with 12 Brüel and Kjær ¼-inch microphones each and two additional stations of 12 loudspeakers are also installed on both sides. The second loudspeakers array is situated after the bends due to a lack of space right downstream of the microphone array. The fan is installed in his volute and connected to the testing duct using a convergent and a diffuser. For all measurements, the fan operates at a constant rotational speed $\Omega = 3000$ rpm, monitored by a diode flush-mounted on the fan casing. The mass flow rate is computed using a Pitot probe, and the total pressure rise of the fan is evaluated by measuring the static pressure increase of the fan between the Pitot and the downstream pressure tap corrected from the losses within the duct using empirical formulas as shown in Eq. 2.

Distortions grids are installed between the convergent and the hot-wire module to generate the various inflows causing installation effects. A constant temperature hot-wire anemometer probe measures the inflow distortions generated by the grid and ingested by the fan 50 mm upstream of the fan inlet. The hotwire is installed on a module actuated by two motors to measure inflow distortion maps as shown in Fig. 2.

The acoustic measurements are performed using the so-called multi-ports technique introduced by Lavrentjev in 1995 [10]. This technique is an extension of the well-known two-port method to higher-order modes [11, 12]. It uses the modal description of the incident and reflected acoustic field to provide a measure of the fan noise emission (respectively noted $\mathbf{p}_{a,b}^{\pm}$ and $\mathbf{p}_{a,b}^s$ in Fig.1). This

allows for induct acoustic measurement free from the artefacts of the duct, such as the superposition of the acoustic field emitted by the fan with the field reflected by the duct terminations and the contamination of the microphones readings by the turbulent boundary layer pressure fluctuations that would contaminate the results otherwise. Several studies have shown the potential of this multi-port approach for the investigation of installations effects in an automotive axial fan [13], in an aircraft environmental control system [14] and domestic appliances applications [15].

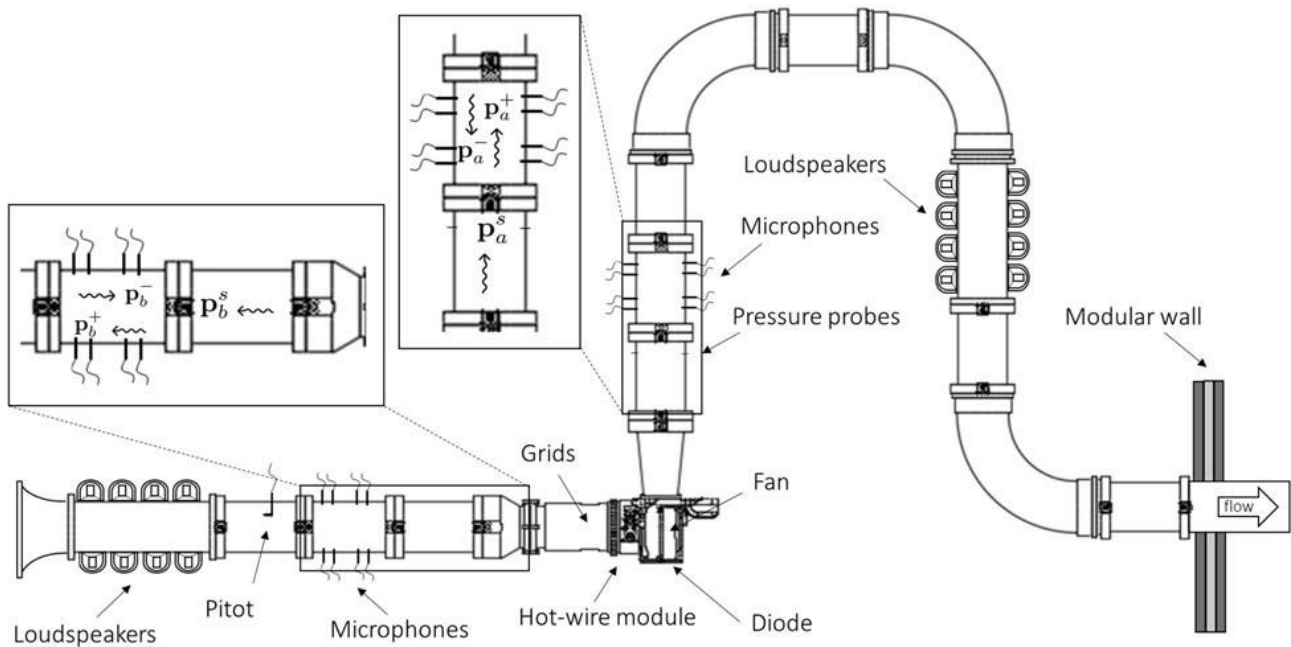


Figure 1: An illustration of the instrumentation of the facility. The vectors \mathbf{p}^+ and \mathbf{p}^- are respectively the incident and outgoing acoustic pressure fluctuations in each mode. The vector \mathbf{p}_s is the source vector. The indices a and b shows the downstream and upstream side of the multi-ports

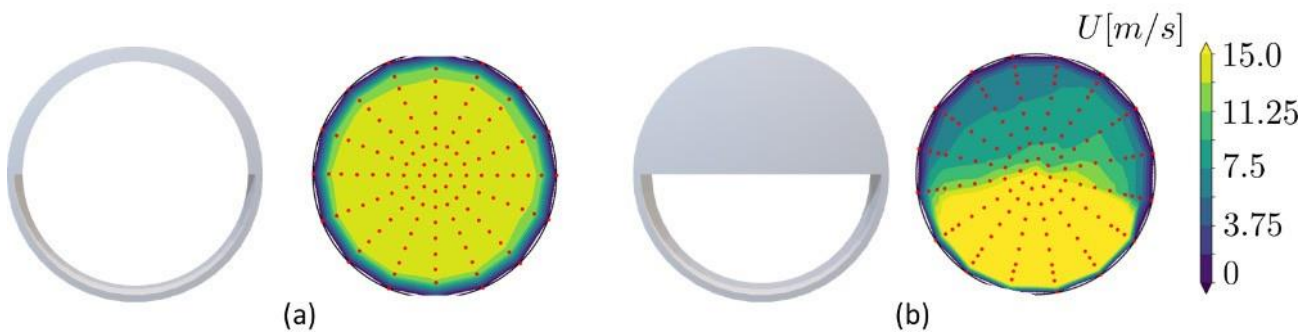


Figure 2: Distortion grids and respective axial velocity map at 50 mm from the fan inlet.
 (a) uniform: an empty duct with small 5% turbulence intensity.
 (b) distorted: a half-moon flow-conditioning grid with large 30% turbulence intensity.

According to Ffowcs Williams and Hawkins analogy [16], the noise generated by a rotating machine can be decomposed into three main components: the thickness noise, the turbulence noise and the loading noise. At low Mach number and for thin rotor blades, the unsteady loading noise dominates the sound production. This loading noise is characterised by broadband and a tonal component. The latter is emitted at the blade passing frequencies $n\Omega B$ (with B being the number of rotor blades) and produced by the unsteady forces acting on the blades [17]. The tonal peak at the first blade passing frequency is identified under uniform inflow but disappeared for the distorted inflow and broadband noise increases of 5 – 7 dB(A) over all frequencies in Fig. 3.

At this stage, we have shown that inflows have a strong impact on fan noise emissions. However, it is not clear which are the dominant noise source mechanisms and how they are impacted by distorted inflows. Therefore, in the next section, we used numerical simulations to investigate in more details the impact of inflows on the different parts of the fan.

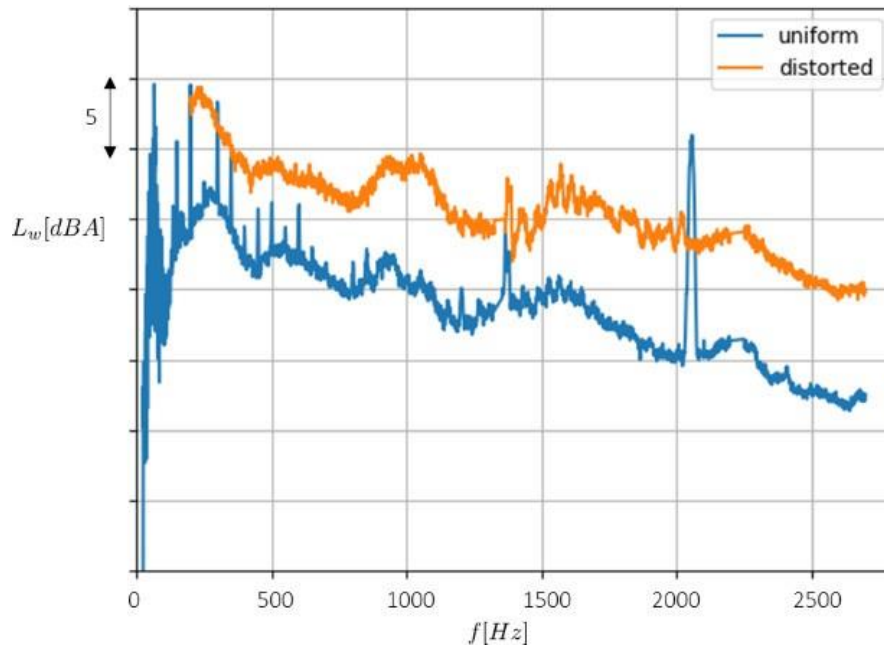


Figure 3: Comparison of the fan noise emission downstream of the fan with uniform and distorted inflow at a mass flowrate $q \approx 580$ kg/h.

SIMULATION MODEL

According to Colonius [18], the methods for computational aeroacoustics (CAA) can be classified into two broad categories: Direct and Hybrid approaches. Direct methods aim at computing both the unsteady flow and the sound generated by it. Unfortunately, those methods are computationally expensive and can only be applied to simple academic flow configurations. In the case of flows at low Mach numbers [19], without back-coupling of the acoustic waves on the flow field, a hybrid workflow for sound propagation can be used. The hybrid workflow relies on three steps (1) perform unsteady flow simulation on a restricted sub-domain that encompasses all acoustic sources (2) compute the acoustic sources from the flow field entities (3) perform a second calculation for predicting the noise and propagating it to the listener in the duct or in the far field.

In this work, we use a compressible LES for the unsteady flow computation on StarCCM+, where the large and energetic scales of turbulence are resolved, and the small and dissipative scales are modeled. Acoustic sources are computed based on the turbulent pressure fluctuations exported from StarCCM+ as *.cgns* files. The propagation of the wave equation will later be performed using a finite element and compared to the experimental measurements.

Geometry

The geometry of interest is plotted in Fig. 4. The CFD simulations account for Valeo's centrifugal fan with 41 blades rotating at 3000 rpm within the testing duct from the experimental campaign. The geometry includes the entire inlet duct with its distortion grids to correctly model the installation effects encountered during the experiments. At the outlet, the duct was truncated before the turn to reduce the size of the computational domain. Because the outlet is situated further than 10 duct diameter from any geometrical singularities, we expect this will not impact the CFD results.

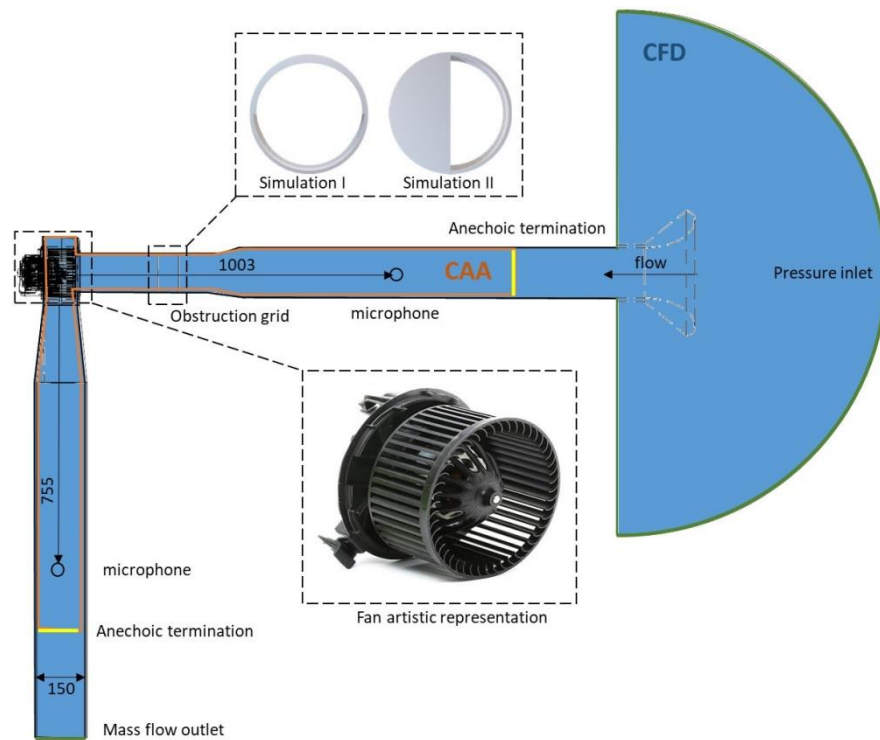


Figure 4: Schematic geometry of the fan and test facility regions. The CFD region used for the LES turbulent flow simulation is highlighted in blue while the Region for the sound propagation is shown in red with all dimensions in mm.

Flow simulation

A large eddy simulation (LES) in combination with the wall-adapting local eddy-viscosity (WALE) subgrid-scale (SGS) model is used to model the turbulent flow. The WALE SGS model is well suited for complex geometries as it accounts for both the strain and rotation rate and does not require tuning of modelling constants for different flow configurations [20]. Using LES, the large and energetic scales of turbulence are resolved, and the small and dissipative scales are modelled. As a result, the dominant noise sources are resolved without any modelling error and provide a reliable basis for acoustic computation.

For discretisation of the convective and diffusive terms, a central difference scheme with a second-order accuracy was used with a time step of 10^{-5} s. It should be noted that this temporal resolution is defined based on the advection speed of the flow, but is not meant to resolve acoustic propagation. A mass flow rate of $q = 580$ kg/h is imposed at the outlet to set the fan operating condition similar to the one from the experimental campaign. Constant static pressure of 0 Pa is imposed at the inlet.

The computational mesh comprises approximately 67×10^6 cells with refinement area around the blades, the casing, and the inlet with the distortion grid. The mesh comprises a polyhedral mesh within the flow and a thin prismatic layer close to the walls to correctly resolve the turbulent boundary layer by keeping a y^+ inferior to 1. The computational domain is divided into two zones, one moving around the rotating impeller and the other stationary. Both zones are coupled via a sliding interface. This meshing size was chosen after a grid refinement study that showed a cut-off frequency of 3500 Hz.

Acoustic sources computation

For this investigation, the focus lies on the noise generated by the fan's blades which are believed to be the most dominant source of noise for fan at low Mach numbers. Following the formulation of Roger and Moreau [17], the tonal noise generated by a subsonic open rotor in the frequency domain at the angular blade passing frequency $\omega = n\Omega B$ can be written as

$$p_{nB}(\mathbf{x}) = \frac{ik_{nB}R'}{4\pi} \sum_{s=-\infty}^{\infty} F_s(r) \left(\cos \theta \cos \gamma(r) G_{nB-s}^{(1)} + \sin \theta \sin \gamma(r) G_{nB-s}^{(2)} \right), \quad (1)$$

$$\text{Where: } G_m^j = \frac{\Omega}{2\pi} \int_0^{2\pi/\Omega} G_j(t) e^{im\Omega t} dt, \quad G_1(t) = \frac{e^{ikR'}}{R'^2} \left[1 - \frac{1}{ikR'} \right], \quad G_2(t) = \sin(\Omega t - \phi) G_1(t).$$

F_s is the complex Fourier coefficient value of force acting on the blade at the blade passing frequency $n\Omega B$ acting as an equivalent rotating dipole. (R, θ, γ) are the spherical coordinate of the listener, and R' is the exact distance between the source and the listener. $k_{nB} = n\Omega B/c_0$ is the wavenumber at the blade loading harmonics

This formulation shows that the driving mechanism of fan noise is the fluctuating blade forces which will be analysed in more details in next section. This rotating dipole formulation is equivalent to a continuous array of circular phased dipoles at the same radius given that the strength of the dipole at angular position α is $F_s e^{in\alpha}$, that the angle of the dipole is the same as the one of the fluctuating lift and the angular frequency of the dipole is $n\Omega B$ [21]. This mathematical representation will be used in the future to model tonal fan noise sources within the finite element solver to account for scattering effects. For the broadband noise, the same phase-shifted dipole representation will be used, only the fluctuating forces and angular frequency are chosen different from the fan rotational frequency.

In the following section, we investigate different installation effects caused by the distorted inflows. Among which, we analyse the impact on the blade loading

INSTALLATION EFFECTS

Fan aerodynamic performances

Figure 5 shows the fan aerodynamic performances are strongly affected by the change of inflow. Because the grid introduces a pressure loss, the difference in total pressure generated by the fan was computed by measuring the difference of static pressure between the upstream and downstream pressure sections in Fig 1 and correcting with empirical values for the pressure loss of the grid, the cone and the duct parts such as :

$$\Delta P_T = \Delta p + \zeta_{diffuser} + \zeta_{duct} + \zeta_{grid} \quad (2)$$

where Δp is the static pressure difference between the Pitot and the downstream pressure probes. $\zeta_{diffuser}$, ζ_{duct} and ζ_{grid} are respectively the pressure losses due to the diffuser, the straight duct parts, and the distortions grids if one is used. The main contributors in Eq. 2 are the fan pressure differential and the grid total pressure loss which is estimated to $\zeta_{grid} \approx 700$ Pa for the half-moon grid at $q = 580$ g/h. The estimation for the grid pressure loss was obtained experimentally by removing the impeller and using the wind tunnel external fan alone to generate the mass flow rate within the duct.

Once the losses are accounted for, we can see that the fan generates a more significant pressure rise under the distorted inflow. Of course, this increase is not enough to compensate for the pressure drop induced by the grid that has been corrected in Fig 5. But this will likely influence the noise generated by the fan as it operates in drastically different conditions. This augmentation of the pressure rise across the fan is surprising as non-uniform inflow was expected to decrease the fan performance in comparison to their nominal operation. Moreover, it was checked that the fan electrical power consumption during the experiments remained unchanged, implying that the distorted inflow resulted in a net fan aerodynamic efficiency rise of approximately 8%. However, this increase in fan total pressure was observed in both the experimental campaign and through simulations. Indeed, computing the pressure rise numerically at the fan's inlet and outlet confirms that it generates a

higher pressure rise in distorted inflow. While this result is surprising, the non-uniform inflow may have accidentally a positive net impact on the fan aerodynamic performances.

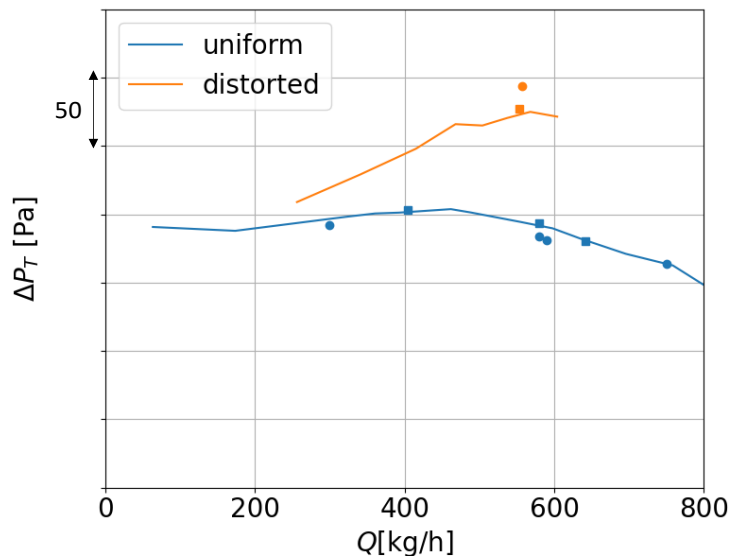


Figure 5: Total pressure performances curves under uniform and distorted inflow. The experimental measurements —, acoustic multi-ports measurements □, URANS simulations •.

Blade loading harmonics

As noted in Eq. 1, the blades loading harmonics are the main acting parameter to subsonic impeller noise. In this section, the influence of distorted inflow on every blade's force is analysed in the time domain by delaying each blade signal with its blade passing frequency $N_i \Delta\theta / \omega$ with N_i being the blade number and $\Delta\theta$ being the angular spacing between two blades. Such processing allows visualizing and separate the periodic blade forces fluctuations responsible for tonal noise generation from the random turbulent contribution responsible for the broadband noise.

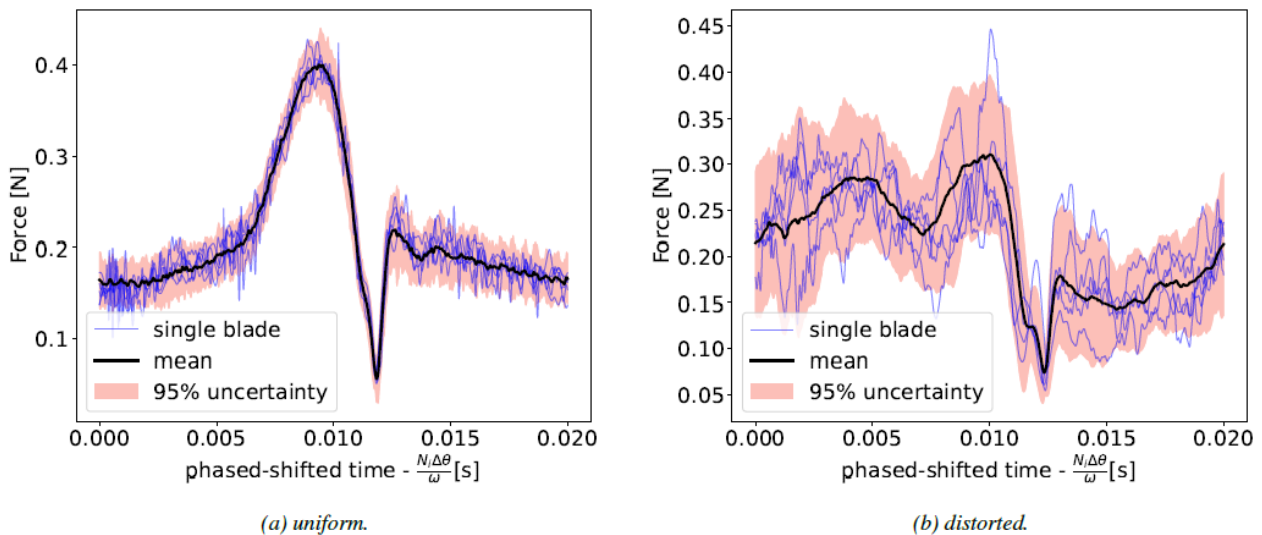


Figure 6: phased-locked time signal of the blades loading's under (a) uniform inflow and (b) distorted inflow

Under uniform inflow, Fig. 6(a) clearly shows the impact of the volute tongue on every blade loading with the rise in the blade's force amplitude prior to the volute's tongue position and its sudden decrease as the blades pass by. Those periodic mean oscillations are the driving mechanism for the fan tonal noise emission. This can also be observed from the evolution of the static pressure inside the fan casing in Fig. 7(a). Indeed, the blade's forces increase corresponds to their passage in

the low static pressure bubble before the volute tongue and their decrease to the static pressure rise in the vicinity of the volute's tongue.

The blade loadings are drastically different under the distorted inflow in Fig. 6(b). The blade loading still decreases after the passage of the volute's tongue but does not show the force's increase prior to that point because the low-pressure region responsible for this increase has disappeared, as shown in Fig. 7(b). It can be also observed that the unsteady force exerted by one blade is not representative anymore of the force history over the other blades. As a result, the acoustic fields emitted by the individual blades are not interfering as constructively, leading to an overall reduction of the tonal noise. Besides, it can be reasonably assumed that the blade-to-blade variations shown in Fig. 6b imply that the force history on any of the blades won't be periodic in time. This increased randomness of the blade loading corresponds to the significant increase of the broadband levels that was measured.

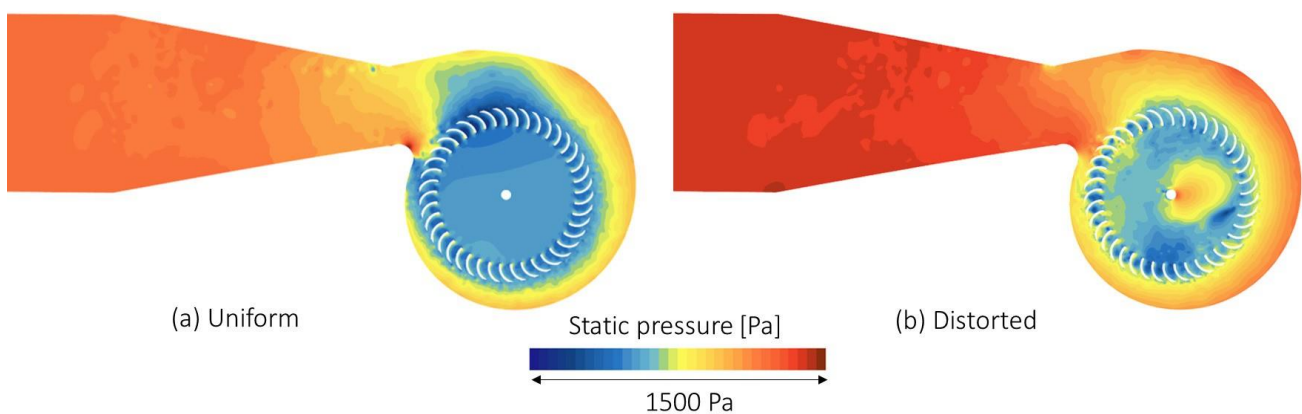


Figure 7: Static pressure distribution in a plane perpendicular to the wheel at 50 % of span in (a) uniform (b) distorted inflow.

Another phenomenon worth noticing is the apparition of another high static pressure region close to the axis of rotation of the wheel where the inflow distortion has its highest speed. We can also observe that if all the blades seem to have a similar loading in uniform inflow, it is not the case when distorted inflow is considered. This implies that to compute the equivalent sources in a numerical approach, one must extract the pressure fluctuation from all the blades to correctly model installation effects.

CONCLUSION AND FUTURE WORK

The experimental campaign performed in the ALCOVES anechoic wind tunnel of the von Karman institute showed that the distorted inflow induced by a half-moon grid situated upstream of the fan led to a severe fan noise increase. The spectral acoustic power highlighted a broadband noise increase of 5-7 dB overall frequencies and a suppression of tonal noise emission at the fan's blade passing frequency. A numerical approach was performed using LES flow simulations for the acoustic sources' computation to unveil the mechanism responsible for this noise increase. According to the FWH analogy, the blades' loading harmonics dominate subsonic fan noise. In uniform inflow, the blade loading harmonics were similar for each blade, with a periodic oscillation in the vicinity of the volute's tongue due to the potential interaction caused by the static pressure rise near the volute tongue, which is likely responsible for the tonal noise generation. In distorted conditions, each blade experience a different blade loading and the impact of the volute's tongue on the potential noise interaction can no longer be observed. The similarity between the measured noise difference under different inflow and the blade loading harmonic suggests that the impeller is responsible for

the acoustic installation effects observed in the experiment. In the future, a comparison of the propagation of the blades' equivalent acoustic sources in a FEM solver with the acoustic measurements will be performed. This will provide valuable insight into the dominating sound generation mechanism in distorted inflow.

REFERENCES

- [1] Europ. Commission, *European green deal*, 2019.
- [2] M.-A. Pallas, J. Kennedy, I. Walker, R. Chatagnon, M. Berengier, and J. Lelong, *Noise emission of electric and hybrid electric vehicles: deliverable FOREVER (n° Forever WP2_D2-1-V4)*. PhD thesis, IFSTTAR-Institut Français des Sciences et Technologies des Transports, de l'Aménagement et des Réseaux, **2015**.
- [3] W. Neise, *Noise reduction in centrifugal fans: a literature survey*, Journal of Sound and Vibration, vol. 45, no. 3, pp. 375–403, **1976**.
- [4] A. Guédel, *Acoustique des ventilateurs: génération du bruit et moyens de réduction*. Ed. PYC Livres, **1999**.
- [5] A. Bolton, *Installation effects in fan systems*, Proceedings of the Institution of Mechanical Engineers, Part A: Journal of Power and Energy, vol. 204, no. 3, pp. 201–215, **1990**.
- [6] B. Mugridge, *Axial flow fan noise caused by inlet flow distortion*, Journal of Sound and Vibration, vol. 40, no. 4, pp. 497–512, **1975**.
- [7] M. Sturm and T. Carolus, *Tonal fan noise of an isolated axial fan rotor due to inhomogeneous coherent structures at the intake*, Noise Control Engineering Journal, vol. 60, no. 6, pp. 699–706, **2012**.
- [8] S. Lee and G.-C. Yang, *Acoustic scaling of an axial fan with non-uniform inlet flows*, KSME International Journal, vol. 13, no. 10, pp. 752–761, **1999**.
- [9] F. J. Krömer, *Sound emission of low-pressure axial fans under distorted inflow conditions*. FAU University Press, **2018**.
- [10] J. Lavrentjev, M. Åbom, and H. Bodén, *A measurement method for determining the source data of acoustic two-port sources*, Journal of sound and vibration, vol. 183, no. 3, pp. 517–531, **1995**.
- [11] J. Lavrentjev and M. Åbom, *Characterization of fluid machines as acoustic multi-port sources*, Journal of Sound and Vibration, vol. 197, no. 1, pp. 1–16, **1996**.
- [12] H. Boden and M. Åbom, *Modelling of fluid machines as sources of sound in duct and pipe systems*, Acta Acustica - Les Ulis, vol. 3, pp. 549–560, **1995**.
- [13] S. Allam and M. Åbom, *Investigation of aerodynamic installation effects for an axial fan*, in 19th AIAA/CEAS Aeroacoustics Conference; Berlin; Germany; 27 – 29 May **2013**.
- [14] M. Shur, M. Strelets, A. Travin, J. Christophe, K. Kucukcoskun, C. F. Schram, S. Sack, and M. Åbom, *Effect of inlet distortions on ducted fan noise*, in 22nd AIAA/CEAS Aeroacoustics Conference, p. 2819, **2016**.
- [15] J. Dominique, J. Christophe, R. Corralejo, and C. Schram, *Multi-port reduction of installation effects applied to a small axial fan*” Acta Acustica united with Acustica, vol. 105, no. 1, pp. 75–85, **2019**.
- [16] J. Ffowcs Williams and D. L. Hawkings, *Sound generation by turbulence and surfaces in arbitrary motion*, Philosophical Transactions for the Royal Society of London. Series A, Mathematical and Physical Sciences, pp. 321–342, **1969**.

- [17] M. Roger and S. Moreau, *Aeroacoustic installation effects in cooling fan systems. Part 1: Scattering by surrounding surfaces*, in Proceedings of the International Symposium on Transport Phenomena and Dynamics of Rotating Machinery, Honolulu, HI, USA, pp. 17–22, **2008**.
- [18] T. Colonius and S. K. Lele, *Computational aeroacoustics: progress on nonlinear problems of sound generation*, Progress in Aerospace sciences, vol. 40, no. 6, pp. 345–416, **2004**.
- [19] S. Schoder, M. Weitz, P. Maurerlehner, A. Hauser, S. Falk, S. Kniesburges, M. Döllinger, and M. Kaltenbacher, *Hybrid aeroacoustic approach for the efficient numerical simulation of human phonation*, The Journal of the Acoustical Society of America, vol. 147, no. 2, pp. 1179–1194, **2020**.
- [20] F. Nicoud and F. Ducros, *Subgrid-scale stress modelling based on the square of the velocity gradient tensor*, Flow, turbulence and Combustion, vol. 62, no. 3, pp. 183–200, **1999**.
- [21] M. Roger and S. Moreau, *Tonal-noise assessment of quadrotor-type uav using source-mode expansions*, in Acoustics, vol. 2, pp. 674–690, Multidisciplinary Digital Publishing Institute, **2020**.